


Magnetic field induced phases in CuCrO_2 : Monte Carlo and analytical investigationsDenis Ledue,^{1,*} Warren Logi Ndzamba,¹ Renaud Patte¹ and Ahmed Albaalbaky²¹Normandie Université, UNIROUEN, INSA Rouen, CNRS, GPM, F-76800 Saint Étienne du Rouvray, France²Université de Nantes, CNRS, Institut des Matériaux Jean Rouxel, IMN, F-44000 Nantes, France (Received 22 October 2020; revised 29 January 2021; accepted 15 February 2021; published 1 March 2021)

Motivated by the strong magnetoelectric coupling in the multiferroic geometrically frustrated triangular antiferromagnet CuCrO_2 and the high sensitivity of its magnetic structure to external fields, we investigate induced magnetic phases at very low temperatures under high magnetic fields (B) up to 325 T applied along the [001] direction. Analytical calculations and Monte Carlo (MC) simulations based on a realistic three-dimensional classical Heisenberg model are used to reveal these magnetic phases. Interestingly, our model mimics a real distorted crystal which considers exchange interactions up to third-nearest neighbors in the ab plane and an interplane interaction, in addition to hard and easy axes anisotropies along the [110] and the [001] directions, respectively. For $B \geq 70$ T, both our MC and analytical results are in an excellent agreement and evidence three commensurate phases, namely, the commensurate Y (CY), the up-up-down (UUD), and the V phases as the magnetic field increases. The field dependence of the characteristic angles of the CY and V phases is determined. Moreover, the saturation field is estimated at 325 T, indicating that the previously predicted values obtained by extrapolation of experimental data are too small. Below 70 T, our MC results indicate that the CY phase is no more stable and several incommensurate Y phases appear. Overall, the observed magnetic phases at nearly 0 K are in a good agreement with a recently published experimental phase diagram. It should be noted that our MC data reject the incommensurate umbrella phase at very low temperatures, which was reported in previous studies.

DOI: [10.1103/PhysRevB.103.094401](https://doi.org/10.1103/PhysRevB.103.094401)**I. INTRODUCTION**

Multiferroics are materials that exhibit more than one ferroic property in the same phase (ferromagnetism, antiferromagnetism, ferroelectricity, antiferroelectricity, ferroelasticity...). Recently, these materials have become one of the hottest topics in condensed matter physics and materials science because they bring out novel physical phenomena and pave the way for new multifunctional materials. Ferroelectricity can be induced by unconventional magnetic ordering that arises from geometrical magnetic frustration and breaks spatial inversion symmetry in crystals [1–3]. Since frustrated structures are highly sensitive to external fields and any changes in the magnetic structure can alter the ferroelectricity, the application of magnetic fields plays an important role in elucidating new magnetic and ferroelectric phases in these compounds. An important member of the multiferroic family is the delafossite oxide CuCrO_2 ($R\bar{3}m$ space group), which possesses a strong magnetoelectric coupling observed in the magnetically ordered state below $T_N = 24 - 27$ K [4–7]. The magnetic structure below T_N is incommensurate proper screw with a propagation vector $\mathbf{q} = (0.329, 0.329, 0)$ pointing along the [110] direction [6,8–10]. Upon spiral magnetic ordering, a tiny in-plane lattice distortion of the order of 0.01% takes place, leading to two different nearest-neighbor (NN) exchange interactions [11,12], and a hard axis anisotropy along the [110] direction [7,10]. Such lattice deformation breaks

the crystal spatial inversion symmetry and thus induces a spontaneous electric polarization along the [110] direction. Interestingly, experimental and numerical investigations revealed a very rich $H - T$ phase diagram in CuCrO_2 with several magnetic and ferroelectric phases when applying $\mathbf{H} \parallel [001]$ [13–19]. A transition in the electric polarization was observed near 45 T and has been attributed to the same proper screw-type spiral to a cycloidal-spiral transition that occurred at 5.3 T when $\mathbf{H} \parallel ab$ plane [16]. Further measurements of electric polarization up to 92 T have provided additional information about the existent phase transitions [17]. Two years later, nuclear magnetic resonance measurements in a magnetic field up to about 45 T along the [001] direction were carried out in the temperature range $2 \leq T \leq 40$ K [18]. It was found that a three-dimensional (3D) magnetic ordering takes place in the low field range (≤ 15 T). At higher magnetic fields, the directions of the magnetic moments from neighboring planes are not correlated, reflecting a two-dimensional (2D) behavior. It was established that the 2D–3D transition is hysteretic in field and temperature. More recently, a magneto-optical study of CuCrO_2 has been carried out in ultrahigh magnetic fields $\mathbf{H} \parallel [001]$ up to 120 T and at temperatures down to 5 K [19]. At temperatures around 10 K, an up-up-down (UUD) magnetic phase was observed in the range 90–105 T, and the Y and V phases (Fig. 1) were proposed to be the adjacent phases, below 90 T and above 105 T, respectively. At 5 K, they observed a first-order phase transition at 76 T which was previously detected too [17].

Numerical investigations were also carried out using a simplified 2D model that considers intralayer exchange

*denis.ledue@univ-rouen.fr

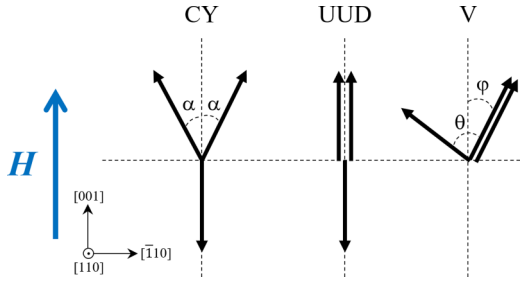


FIG. 1. Magnetic moment configurations in the commensurate Y (CY), the up-up-down (UUD), and the V phases seen in CuCrO_2 .

parameters up to third neighbors [15]. This model predicts a three-sublattice state with a magnetization equal to one-third of the saturated value at ~ 90 T. More recently, a Monte Carlo (MC) study based on a minimal model including spatially anisotropic NN interactions and single ion anisotropy terms was done [17]. However, an artificial large lattice distortion corresponding to $J_{[100]}/J_{[110]} = 0.7654$ was used which provides a propagation vector $\mathbf{q} = (0.3125, 0.3125, 0)$ noticeably deviated from the experimental one $\mathbf{q} = (0.329, 0.329, 0)$ [6]. For $\mathbf{H} \parallel [001]$, they obtained the following equilibrium phases as a function of increasing field: incommensurate Y (ICY), incommensurate umbrella (ICU), incommensurate Y (CY), UUD, V, and, finally, ICU. They found that the UUD phase exists even at low temperatures when \mathbf{H} is parallel to the easy axis and it becomes stable roughly at 1/3 of the saturation field. Among these phases, it is noticeable that only the ICU phase is noncoplanar. However, this model suffers from considering only NN exchange interactions and neglecting interplane interactions. Consequently, further numerical investigations with an extended model are still needed to better understand experimental data and provide precise clarifications at largely applied magnetic fields.

In this paper, we investigate the magnetic field induced phases in CuCrO_2 by means of analytical calculations and MC simulations. Our model is more realistic than previous ones [15,17] since it considers exchange interactions up to the third neighbors in the ab plane and interplane interactions

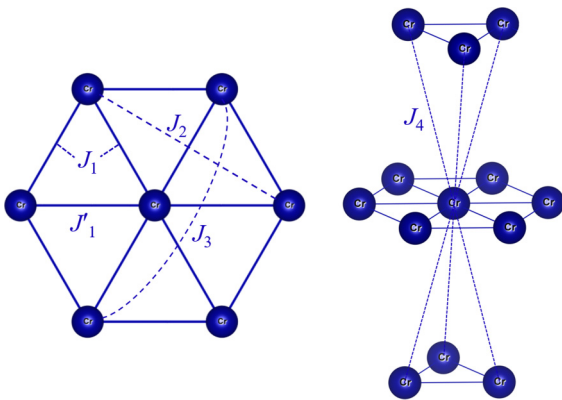


FIG. 2. Schematic representation of the intraplane exchange interactions within the ab plane (J_1 is along $[100]$ and $[010]$, and J'_1 is along $[110]$ with $|J_1/J'_1| < 1$) and the interplane exchange interaction J_4 .

TABLE I. Numerical values (in K) of the magnetic parameters reported in Ref. [20].

J'_1/k_B	J_1/k_B	J_2/k_B	J_3/k_B	J_4/k_B	D_x/k_B	D_z/k_B
-30.314	-27.788	0.14	-3.088	-0.702	-0.008	0.379

(Fig. 2) as well as single ion anisotropy axes. The values of the exchange interactions and single ion anisotropy constants used were estimated using first-principles calculations in our previous study [20]. These parameters were checked against the experimental Néel and Curie-Weiss temperatures as well as the electric coercive field, thereby proving them to be good candidates to model the magnetoelectric properties of CuCrO_2 [7]. We calculate analytical expressions of the magnetic energy of the CY, UUD, V, and ferromagnetic (FM) phases to analyze our MC results and to confirm or infirm previous numerical or experimental data [16–19].

The remainder of this paper is organized as follows: Section II presents the model and simulation details. Section III is devoted to discussions of the analytical and MC results, and, finally, a conclusion is given in Sec. IV.

II. MODEL AND SIMULATION

A. Model

To model the magnetic field induced phases in CuCrO_2 , we only consider Cr^{3+} ions with $S = 3/2$ since Cu^+ and O^{2-} are nonmagnetic. We consider the following classical 3D Hamiltonian including the Heisenberg exchange term, single ion anisotropy terms and the Zeeman term:

$$H = - \sum_{(i,j)} J_{ij} \mathbf{S}_i \cdot \mathbf{S}_j - D_x \sum_i (S_i^x)^2 - D_z \sum_i (S_i^z)^2 + g\mu_B \mathbf{B} \cdot \sum_i \mathbf{S}_i, \quad (1)$$

where J_{ij} stands for exchange integrals up to fourth neighbors (Fig. 2). The x and z axes correspond to the $[110]$ and $[001]$ directions, respectively. $D_x < 0$ and $D_z > 0$ refer to the single ions anisotropy constants for the hard- and easy-axis anisotropy, respectively. The last term corresponds to the Zeeman energy where \mathbf{B} is the applied magnetic field (μ_B is the Bohr magneton and $g = 2$ is the Landé factor). The numerical values of the magnetic parameters that we use are reported in Table I. They provide a propagation vector $\mathbf{q} = (0.3264, 0.3264, 0)$ very close to the experimental one [20]. It has to be noted that relative to the value of the exchange interaction along $[110]$, our anisotropy constants ($|D_x/J'_1| = 3 \times 10^{-4}$ and $|D_z/J'_1| = 1.25 \times 10^{-2}$) are smaller than those of Ref. [17] ($|D_x/J_{[110]}| = 5 \times 10^{-3}$ and $|D_z/J_{[110]}| = 5 \times 10^{-2}$).

B. Simulation details

Our simulations are performed on 3D lattices of $L \times L \times L_z$ unit cells ($3L^2L_z$ spins) with periodic boundary conditions (PBCs). To simulate the ground state (GS) configuration, we perform a simulated annealing from $T_0 = 30$ K above T_N down to 10^{-4} K following a geometric law $T_{n+1} = \tau T_n$ (with

$0 < \tau < 1$ being the cooling rate) using the MC method [21]. Between T_0 and $T^* = 10$ K, we use the standard Metropolis algorithm [22], whereas below T^* , we use the Metropolis algorithm combined with the time-step-quantified MC method [23,24] to improve the convergence to the GS. During the simulation, we store the magnetic configuration which has the lowest energy ($E_{\text{GS}}^{\text{sim}}$) since it should correspond to the GS configuration of the *finite* crystal. To see whether the magnetic moments of each *ab* plane of this latter configuration are coplanar, we compare for each *ab* plane the two quantities

$$u = \sum_i \|\mathbf{S}_i \times \mathbf{S}_{i+1}\| \quad (2)$$

and

$$v = \left\| \sum_i \mathbf{S}_i \times \mathbf{S}_{i+1} \right\|, \quad (3)$$

where i runs over the spins of the considered *ab* plane. If these two quantities are equal, it means that the magnetic moments of the considered *ab* plane are coplanar with $\mathbf{n} = (\sum_i \mathbf{S}_i \times \mathbf{S}_{i+1})/v$ is the normal unit vector of the plane which contains the magnetic moments. We also calculate the angles θ_a and θ_b between two NN magnetic moments along the [100] and [010] directions, respectively. These angles determine the orientation of each sublattice relative to the others.

We would like to emphasize that, using PBCs, the simulated GS configuration, i.e., the GS configuration in the *finite* crystal, can be slightly different than the true one, i.e., the GS configuration in the *infinite* crystal. Indeed, if the period of the true GS configuration is $\lambda_a, \lambda_b, \lambda_c$ in the \mathbf{a}, \mathbf{b} and \mathbf{c} directions, respectively, the crystal size in the \mathbf{u} direction (with $\mathbf{u} \equiv \mathbf{a}, \mathbf{b}$ or \mathbf{c}) L_u should be a multiple of λ_u (the simulation box should contain a whole number of magnetic unit cells). Otherwise, the energy per spin of the true GS configuration is larger in the *finite* crystal than in the *infinite* one E_{GS}^{∞} because of an excess of energy at the surfaces. To illustrate this point, let us consider the triangular lattice with only NN interactions $J_1 < 0$. In that case, the GS configuration in the *infinite* triangular lattice is the 120° configuration [$\mathbf{q} = (1/3, 1/3)$] with an energy per spin $E_{\text{GS}}^{\infty}/(k_B S^2) = -41.682$ K (for $J_1/k_B = -27.788$ K). In Fig. 3, we plot the size dependence of the energy per spin of this 120° configuration in the *finite* triangular lattice $E_{120^\circ}(L)$. It can be seen that $E_{120^\circ}(L)$ is equal to E_{GS}^{∞} only if L is a multiple of 3 as expected since $3a$ is the period along the \mathbf{a} and \mathbf{b} directions of the 120° configuration. Otherwise, there is an excess of energy at the edges due to PBCs, which decreases as L increases. Consequently, the GS configuration in a *finite* triangular lattice of size L which is not a multiple of 3 is not the 120° configuration. For example, if $L = 22$, the energy per spin is minimum for $k = 0.31818$ [$\mathbf{q} = (k, k, 0)$] as shown in Fig. 4, which is the nearest value to $1/3$ that satisfies the condition kL is an integer ($0.31818 \times 22 \approx 7$). Then, if one performs a simulation with $L = 22$, it will converge to the $k = 0.31818$ configuration. Consequently, the simulated GS energy per spin $E_{\text{GS}}^{\text{sim}}(L)$ can be written as $E_{\text{GS}}^{\text{sim}}(L) = E_{\text{GS}}^{\infty} + \delta E(L)$, where $\delta E(L) \geq 0$ is the energy difference between the true GS and the simulated

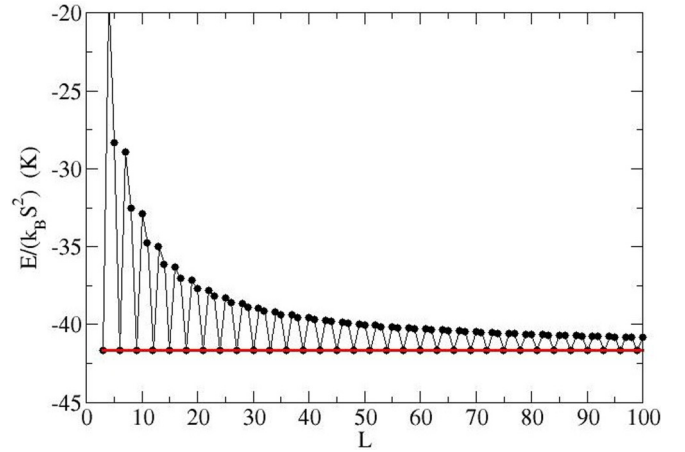


FIG. 3. Size dependence of the energy per spin of the 120° magnetic configuration [$\mathbf{q} = (1/3, 1/3)$] in a *finite* triangular lattice [the energy per spin of the 120° configuration in the *infinite* triangular lattice, $E_{\text{GS}}^{\infty}/(k_B S^2) = -41.682$ K, is shown by the red horizontal line].

one when the simulation box does not contain a whole number of magnetic unit cells [here, $\delta E(L = 22)/(k_B S^2) = 0.398$ K].

III. RESULTS AND DISCUSSIONS

A. Analytical calculations of the energy of the commensurate phases (CY, UUD, V, and FM)

To identify the simulated phases, it is very useful to compare the simulated GS energy $E_{\text{GS}}^{\text{sim}}(L)$ with the energies of the CY, UUD, V, and FM phases. In addition, in the case of the V and CY phases, we can also compare the simulated angles with the theoretical ones.

In the CY phase, one sublattice magnetization is along [001] in the opposite direction of the external field and the other two sublattice magnetizations make the same angle, that we denote α , with [001] (Fig. 1). Then, the energy per spin of

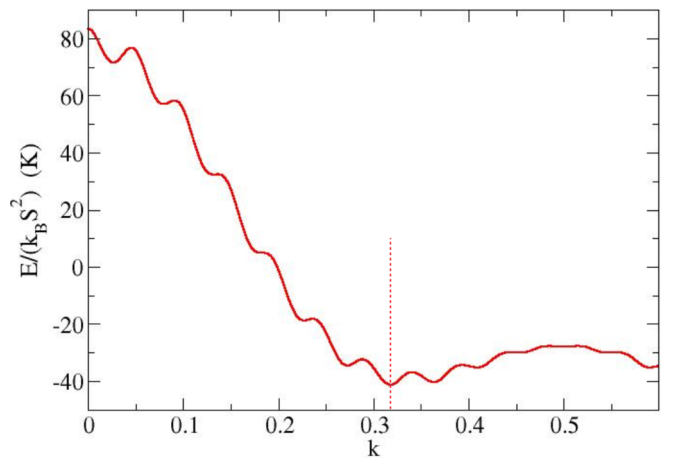


FIG. 4. Energy per spin variation of the magnetic configuration of propagation vector $\mathbf{q} = (k, k, 0)$ versus k in a *finite* triangular lattice of size $L = 22$ (the vertical dashed line indicates the location of the minimum corresponding to $k = 0.31818$).

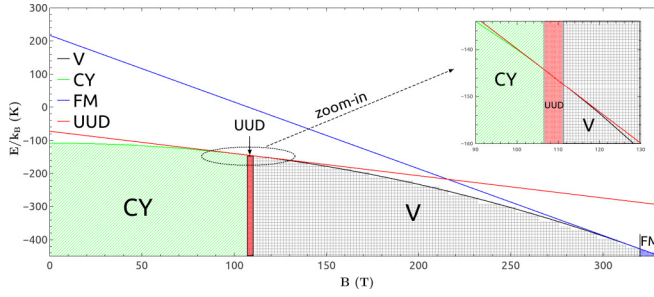


FIG. 5. Energy per spin of the various commensurate phases (CY, UUD, V, and FM) versus the applied magnetic field. Note that the energy of the UUD and FM phases decreases linearly as the magnetic field increases.

this phase is given by

$$E_{CY} = S^2 \left[\left(\frac{2(J_1 + J_4) + J'_1}{3} + J_3 \right) (2\cos(\alpha) - \cos(2\alpha)) - 3J_2 - J_4 - \frac{D_z}{3} (1 + 2\cos^2(\alpha)) \right] + \frac{g\mu_B SB}{3} (1 - 2\cos(\alpha)). \quad (4)$$

Note that the anisotropy energy due to D_x is zero since the spins lie in the yz plane (perpendicular to $[110]$) to minimize this anisotropy energy. The UUD phase is the limit of the CY phase when $\alpha \rightarrow 0$ (Fig. 1), i.e., two sublattice magnetizations are in the same direction as the field and the other one is opposite to the field. Then the energy per spin of the UUD phase is

$$E_{UUD} = S^2 \left[\frac{2J_1 + J'_1 - J_4}{3} - 3J_2 + J_3 \right] - D_z S^2 - \frac{g\mu_B SB}{3}. \quad (5)$$

In the V phase, two sublattice magnetizations are parallel to each other and make an angle φ with $[001]$ and an angle θ with the third sublattice magnetization (Fig. 1). Then, the energy per spin in this phase can be written as

$$E_V = -S^2 \left[(1 + 2\cos(\theta)) \left(\frac{2J_1 + J'_1}{3} + J_3 \right) + 3J_2 + \frac{J_4}{3} (4\cos(\theta - 2\varphi) + 4\cos(2\varphi) + \cos[2(\theta - \varphi)]) \right] - \frac{D_z S^2}{3} (2\cos^2(\varphi) + \cos^2(\theta - \varphi)) - \frac{g\mu_B SB}{3} (2\cos(\varphi) + \cos(\theta - \varphi)). \quad (6)$$

The UUD phase is the limit of the V phase when $\varphi \rightarrow 0$ and $\theta \rightarrow \pi$. Moreover, the FM phase is the limit of the V phase when φ and $\theta \rightarrow 0$, so one obtains

$$E_{FM} = S^2 [2J_1 + J'_1 + 3(J_2 + J_3 + J_4) + D_z] - g\mu_B SB. \quad (7)$$

Note that the energies of the CY and V phases are extracted from a minimization of E_{CY} versus α , and E_V versus φ and θ . In Fig. 5, we plot the theoretical energy of the different phases (V, UUD, CY, and FM) versus the applied magnetic field. It can be seen that below 106 T, the CY phase (with

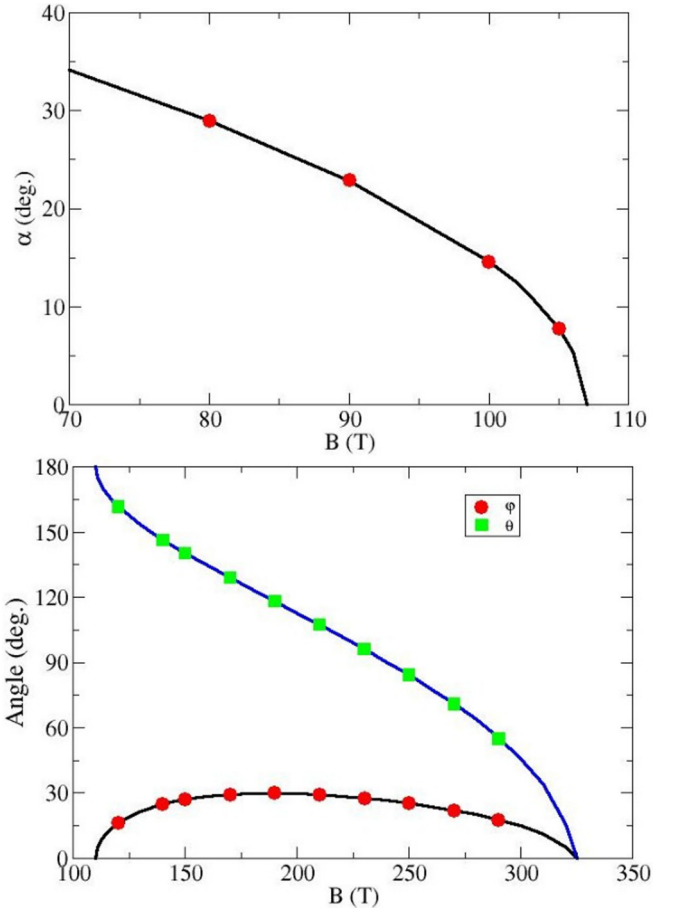


FIG. 6. Magnetic field dependence of α (CY phase), and φ and θ (V phase). Continuous lines represent the theoretical values and filled symbols indicate the MC values.

$\alpha \neq 0$) is the most stable among these four phases. For $107 \text{ T} \leq B \leq 110 \text{ T}$, only the UUD phase exists because (i) $\alpha \rightarrow 0$ as $B \rightarrow 107^- \text{ T}$ (see Fig. 6), which means that the CY phase becomes the UUD phase, and (ii) $\varphi \rightarrow 0$ and $\theta \rightarrow 180^\circ$ as $B \rightarrow 107^+ \text{ T}$ (see Fig. 6), which means that the V phase becomes the UUD phase, so the UUD phase is stable between 107 T and 110 T. In the range $111 \text{ T} \leq B \leq 320 \text{ T}$, the most stable phase is the V phase (with $\varphi \neq 0$ and $\theta \neq 180^\circ$), while the saturation is reached (FM phase) for $B \geq 325 \text{ T}$. More clearly, the stability of these phases can be seen in the magnetic field dependence of the theoretical values of the angles α (CY phase), and φ and θ (V phase) given in Fig. 6. In the V phase, θ decreases monotonically from 180° (UUD) to 0° (FM) as B increases, whereas φ reaches a maximum value of 30° at $B = 190 \text{ T}$.

B. Monte Carlo results

As mentioned in Sec. II B, the choice of size L is essential to simulate the true GS configuration. We select $L = 49$ that is the smallest size for which $kL = 0.3264 \times 49 = 16$ is an integer, and $L = 12$ which is convenient for simulating the commensurate phases. For L_z , we choose the smallest value which is compatible with the PBC along the $[001]$ direction, i.e., $L_z = 2$ according to Ref. [20]. For each simulation,

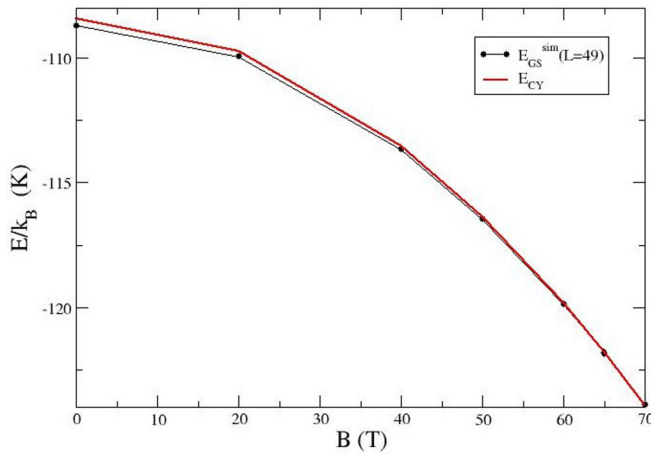


FIG. 7. Comparison of the simulated GS energy per spin $E_{\text{GS}}^{\text{sim}}(L = 49)$ with the energy per spin of the CY phase versus the applied magnetic field for $B \leq 70$ T.

we consider a very slow cooling strategy ($\tau = 0.96$ or 0.98) where 5×10^3 MC steps are performed at each temperature. For each value of B , MC simulations are repeated several times starting from different initial magnetic configurations where we check their convergence to the same GS configuration.

To identify the simulated phase at ~ 0 K, we compare the simulated GS energy $E_{\text{GS}}^{\text{sim}}$ with the theoretical energies E_{CY} , E_{UUD} , E_{V} , and E_{FM} of each phase up to a relative precision of 10^{-5} . We also extract the angles θ_a and θ_b during the simulations which allow determining the orientation of each sublattice relative to the others and consequently the nature of the simulated phase. Finally, we verify the coplanarity of the magnetic moments based on the two quantities u and v [Eqs. (2) and (3)] given in Sec. II B.

For $B \geq 70$ T, numerical simulations with $L = 12$ converge to one of the four commensurate phases: the CY phase for $70 \text{ T} \leq B \leq 106 \text{ T}$, the UUD phase for $107 \text{ T} \leq B \leq 110 \text{ T}$, the V phase for $111 \text{ T} \leq B \leq 320 \text{ T}$, and the FM phase for $B \geq 325 \text{ T}$. The magnetic field dependence of the simulated angles α , φ , and θ are in excellent agreement with the theoretical values as seen in Fig. 6. Consequently, our simulated phase diagram at very low temperatures ($T \approx 0$ K) above 70 T is in an excellent agreement with our analytical calculations presented in Fig. 5. It should be noted that the stability range of the CY, UUD, and V phases is in a good agreement with the experimental phase diagram [19]. Also, our MC simulations provide a saturation field around ~ 325 T which is larger than the experimentally predicted one 270 T [16] and 280 T [18].

For $B \leq 65$ T, the simulated GS energy $E_{\text{GS}}^{\text{sim}}$ of a system of $L = 12$ is higher than that of $L = 49$ (Fig. 7). Our simulations with $L = 12$ converge to the CY phase due to PBCs ($E_{\text{GS}}^{\text{sim}}(L = 12) \approx E_{\text{CY}}$). Consequently, since $E_{\text{GS}}^{\text{sim}}(L = 49) = E_{\text{GS}}^{\infty} + \delta E(L = 49) < E_{\text{CY}}$, the energy E_{GS}^{∞} of the stable phase for $B \leq 65$ T is smaller than E_{CY} evidencing that the CY phase is no more stable, and therefore incommensurate Y

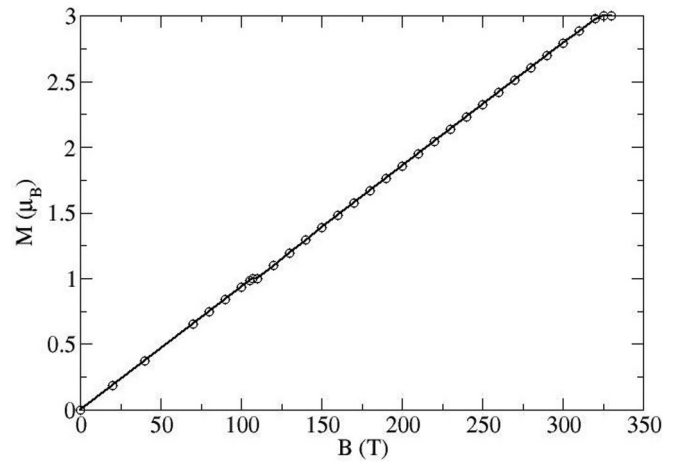


FIG. 8. Applied field dependence of the simulated magnetization per Cr^{3+} ion (in μ_B) at ~ 0 K.

states (ICY) become more stable. Therefore, incommensurate Y phases (ICY) are expected to be stable below 65 T.

For all values of B , the magnetic moments of the simulated GS lie in the yz plane (perpendicular to the $[110]$ direction). Consequently, our MC simulations reject the presence of non-coplanar magnetic phases at very low temperatures contrary to the calculated phase diagram of Ref. [17] where the ICU phase was predicted. In Fig. 8, we plot the applied field dependence of the magnetization per spin M at ~ 0 K. The curve exhibits a linear variation with $M \sim 0.5 \mu_B / \text{Cr}^{3+}$ at 50 T, and a plateau between 107 T and 110 T which corresponds to the UUD phase in agreement with Ref. [17]. However, no clear evidence of such a plateau was seen in Ref. [19]. Importantly, the magnetization per spin tends to its saturated value ($3 \mu_B$) at 325 T.

IV. CONCLUSIONS

In this paper, we investigated the induced magnetic phases in CuCrO_2 at very low temperatures under magnetic fields up to 325 T \parallel $[001]$ direction by means of analytical calculations and MC simulations based on a realistic 3D classical Hamiltonian model. Below 70 T, the incommensurate Y phases are proposed to be the stable phases. For $B \geq 70$ T, several commensurate phases (CY, UUD, V, and FM) seen in this order as the applied field increases were found to be stable confirming the recent published experimental phase diagram [19]. Interestingly, our MC results at ~ 0 K exclude noncoplanar magnetic phases previously predicted by numerical simulations [17]. Moreover, saturation ($M = 3 \mu_B / \text{Cr}^{3+}$) occurs at very high magnetic field around 325 T. Our present paper shows that MC simulations are suited to determine the magnetic field induced phases at very low temperatures, opening up the prospect of the determination of the complete $H - T$ phase diagram of CuCrO_2 and similar compounds.

ACKNOWLEDGMENTS

This project was funded by the Région Normandie and the European Union. Europe invests in Normandy with the Euro-

pean Regional Development Fund (ERDF)–MAGMA project. The authors acknowledge the Centre Régional Informatique et

d’Applications Numériques de Normandie (CRIANN) where simulations were performed as Project No. 2015004.

-
- [1] T. Kimura, T. Goto, H. Shintani, K. Ishizaka, T. Arima, and Y. Tokura, *Nature* **426**, 55 (2003).
 - [2] T. Kimura, J. C. Lashley, and A. P. Ramirez, *Phys. Rev. B* **73**, 220401(R) (2006).
 - [3] S. W. Cheong and M. Mostovoy, *Nat. Mater.* **6**, 13 (2007).
 - [4] T. Okuda, N. Jufuku, S. Hidaka, and N. Terada, *Phys. Rev. B* **72**, 144403 (2005).
 - [5] S. Seki, Y. Onose, and Y. Tokura, *Phys. Rev. Lett.* **101**, 067204 (2008).
 - [6] M. Poienar, F. Damay, C. Martin, V. Hardy, A. Maignan, and G. André, *Phys. Rev. B* **79**, 014412 (2009).
 - [7] A. Albaalbak, Y. O. Kvashnin, D. Ledue, R. Patte, and R. Frésard, *Phys. Rev. B* **96**, 064431 (2017).
 - [8] H. Kadowaki, H. Kikuchi, and Y. Ajiro, *J. Phys.: Condens. Matter* **2**, 4485 (1990).
 - [9] M. Soda, K. Kimura, T. Kimura, M. Matsuura, and K. Hirota, *J. Phys. Soc. Jpn.* **78**, 124703 (2009).
 - [10] M. Frontzek, J. T. Haraldsen, A. Podlesnyak, M. Matsuda, A. D. Christianson, R. S. Fishman, A. S. Sefat, Y. Qiu, J. R. D. Copley, S. Barilo, S. V. Shiryayev, and G. Ehlers, *Phys. Rev. B* **84**, 094448 (2011).
 - [11] K. Kimura, T. Otani, H. Nakamura, Y. Wakabayashi, and T. Kimura, *J. Phys. Soc. Jpn.* **78**, 113710 (2009).
 - [12] M. Poienar, F. Damay, C. Martin, J. Robert, and S. Petit, *Phys. Rev. B* **81**, 104411 (2010).
 - [13] K. Kimura, H. Nakamura, S. Kimura, M. Hagiwara, and T. Kimura, *Phys. Rev. Lett.* **103**, 107201 (2009).
 - [14] H. Yamaguchi, S. Ohtomo, S. Kimura, M. Hagiwara, K. Kimura, T. Kimura, T. Okuda, and K. Kindo, *Phys. Rev. B* **81**, 033104 (2010).
 - [15] R. S. Fishman, *J. Phys.: Condens. Matter* **23**, 366002 (2011).
 - [16] E. Mun, M. Frontzek, A. Podlesnyak, G. Ehlers, S. Barilo, S. V. Shiryayev, and V. S. Zapf, *Phys. Rev. B* **89**, 054411 (2014).
 - [17] S.-Z. Lin, K. Barros, E. Mun, J.-W. Kim, M. Frontzek, S. Barilo, S. V. Shiryayev, V. S. Zapf, and C. D. Batista, *Phys. Rev. B* **89**, 220405(R) (2014).
 - [18] Yu. A. Sakhratov, L. E. Svistov, P. L. Kuhns, H. D. Zhou, and A. P. Reyes, *Phys. Rev. B* **94**, 094410 (2016).
 - [19] A. Miyata, O. Portugall, D. Nakamura, K. Ohgushi, and S. Takeyama, *Phys. Rev. B* **96**, 180401(R) (2017).
 - [20] A. Albaalbak, Y. O. Kvashnin, R. Patte, and D. Ledue, *Phys. Rev. B* **99**, 104415 (2019).
 - [21] D. P. Landau and K. Binder, *A Guide to Monte Carlo Simulations in Statistical Physics* (Cambridge University Press, Cambridge, England, 2008).
 - [22] N. Metropolis, A. W. Rosenbluth, M. N. Rosenbluth, A. H. Teller, and E. Teller, *J. Chem. Phys.* **21**, 1087 (1953).
 - [23] U. Nowak, R. W. Chantrell, and E. C. Kennedy, *Phys. Rev. Lett.* **84**, 163 (2000).
 - [24] O. Chubykalo, U. Nowak, R. Smirnov-Rueda, M. A. Wongsam, R. W. Chantrell, and J. M. Gonzalez, *Phys. Rev. B* **67**, 064422 (2003).